Interpretation of phase and strain contrast of TEM images of $In_xGa_{1-x}As/GaAs$ quantum dots

M. De Giorgi,[1] A. Taurino,[1,*] A. Passaseo,[1] M. Catalano,[2] and R. Cingolani[1]
[1]*Istituto Nazionale Fisica della Materia (INFM), Dipartimento di Ingegneria dell'Innovazione, Università di Lecce, 73100 Lecce, Italy*
[2]*Istituto CNR-IME, Consiglio Nazionale delle Ricerche, via Arnesano 73100 Lecce, Italy*
(Received 14 June 2000; revised manuscript received 12 February 2001; published 22 May 2001)

Transmission electron microscopy (TEM) observations were performed on capped single and vertically stacked $In_{0.5}Ga_{0.5}As/GaAs$ quantum dots. Cross-sectional images were obtained both in the ⟨001⟩ and ⟨011⟩ zone axes. In the ⟨011⟩ zone axis the dots exhibit a lens shape, whereas in the ⟨001⟩ zone axis their shape is more likely to be a truncated pyramid or a truncated cone. We demonstrate that, due to the chemical sensitivity of the ⟨001⟩ zone axis, it is possible to distinguish, from the phase contrast features of high-resolution TEM (HRTEM) images, the regions where In is located and consequently get more reliable information about the dot shape. By performing HRTEM simulations, we discuss the experimental conditions under which the compositional signal is observable. [100] plan-view samples were investigated by conventional TEM in the multibeam zone axis condition. The contrast features of the images were correlated to the strain fields in the three-dimensional islands. We show that the different diffraction contrast observed in our samples is due to coherent superposition of the strain field of dots having different sizes along the stack.

DOI: 10.1103/PhysRevB.63.245302 PACS number(s): 68.37.Lp, 68.65.−k, 68.35.Dv

I. INTRODUCTION

The continuous search for improved electronic and optical performances of semiconductor devices has stimulated the study of quantum dots (QD's).[1,2] Different techniques have been used for their fabrication. Among these, the self-assembled growth has been proven to be particularly successful[3,4] as it allows the reproducible realization of quasi-zero-dimensional semiconductors of excellent structural quality. Dots stacked in vertically organized columns are required to increase the optical density of the active medium and to change the emission wavelength.[5] Their size and shape are critical parameters for controlling the optoelectronic properties of the devices.[6] In fact, the ground-state and excited-state emission as well as the intersublevel transitions strongly depend on these parameters. In order to tailor new devices based on such nanostructures, it is crucial to control the shape of the dots and the extent of the wave-function confinement. To this aim, different structural techniques are used, such as atomic force microscopy[7] AFM, scanning tunneling microscopy[8] (STM), and transmission electron microscopy[9] (TEM). The AFM and STM techniques are commonly used to study uncapped quantum dots, whereas the TEM investigation is fundamental to obtain structural information on capped quantum dots, i.e., on real devices. In particular, two-beam and on-zone multibeam plan-view images are routinely used to investigate such structures.[10–14] In spite of the great deal of information that can be derived, the interpretation of the diffraction contrast from such images is very difficult, due to the convolution of strain contrast and composition-dependent contrast. This makes the experimental determination of the QD's shape still rather controversial.[8,13,15,16] Theoretical calculations are often used in order to evaluate the contribution of the strain field to the TEM images as opposed to the compositional Z-dependent contrast. To this aim, sophisticated algorithms, generally based on finite element analyses, are used, in which the strain field is firstly modeled, and the electron diffraction contrast images are then calculated.[17–21] Besides their complexity, these methods need an *a priori* assumption about the dot shape, size, and chemical composition.

Cross-sectional high-resolution images can be used to obtain further experimental data to be introduced, as input parameters, in the theoretical simulations. The current literature shows that much information about the shape and size of the dots is generally deduced from cross-sectional high-resolution TEM (HRTEM) images obtained in the ⟨011⟩ zone axis.[11,22] Nevertheless, much care is required in the interpretation of these images, since the strain contrast is overlapped to the phase contrast and no structural difference between dots and matrix is observed in the ⟨011⟩ zone axis. The effects of the strain relaxation due to the specimen thinning to reach electron transparency must also be taken into account.[23]

In this paper the issue of the chemical and strain contribution to, respectively, the HRTEM cross-sectional and plan-view diffraction contrast images is addressed by a detailed TEM investigation performed on $In_xGa_{1-x}As/GaAs$ quantum dots. This work is separated in two sections. In Sec. III we try to elucidate the results of a HRTEM investigation of a stacked $In_xGa_{1-x}As/GaAs$ quantum-dot heterostructure. We discuss and compare the cross-sectional HRTEM images of a six-fold stacked $In_{0.5}Ga_{0.5}As/GaAs$ quantum dot specimen, obtained in both ⟨001⟩ and ⟨011⟩ zone axes. Finally, we support our results with high-resolution image simulations. In Sec. IV we show the plan-view images obtained from single and vertically stacked quantum dot samples. A correlation between the TEM diffraction contrast and the localized strain field of the single and vertically stacked dots is proposed in order to explain the contrast differences between single and stacked dot images. We show that in the vertically stacked dots, the strain fields associated with dots belonging to different layers coherently superpose along the stack. If the size of the dots in the stack varies, such superposition induces a modulation of the total strain field, resulting in a modification of the electron-diffraction conditions.

 ©2001 The American Physical Society

II. EXPERIMENTAL

The samples under study consist of $In_xGa_{1-x}As/GaAs$ single and six-fold stacked quantum dots grown by metal-organic chemical vapor deposition (MOCVD) on (100) exactly oriented GaAs substrates by the well-known Stranski-Krastanov method. The growth was performed by a horizontal LP-MOCVD reactor (AIXTRON 200 AIX), operating at 20 mbar. Trimethyl gallium (TMGa), trimethyl indium (TMIn), and pure arsine (AsH_3) were used as source materials; palladium purified H_2, with a flow rate of 7 slm, was used as carrier gas. The nominal In/Ga ratio was chosen equal to 0.5. After the growth of 100 nm of an undoped GaAs buffer layer, the dots were grown by depositing 4 monolayers (ML's) of $In_xGa_{1-x}As$; in the stacked samples the dots were separated by GaAs spacers, 5 nm thick. Finally a GaAs cap layer, 30 nm thick, was deposited after a growth interruption time of 60 s under the AsH_3 flow. Further details about the growth conditions are reported elsewhere.[24]

TEM investigations were performed by using a JEOL 4000 EX electron microscope, with an interpretable resolution limit of 0.16 nm. Cross-sectional specimens were prepared by mechanical grinding down to about 100 μm, dimple grinding down to less than 10 μm; finally the electron transparency was reached by ion milling with 4 kV Ar^{2+} ions. Since the angle between the $\langle 001\rangle$ and $\langle 011\rangle$ zone axes is 45° and the typical inclination angles of a high-resolution transmission electron microscope are about $\pm 20°$, the cross-sectional specimens were prepared by gluing face-to-face two slices of samples rotated by 45°, one with respect to the other.

[100] plan-view images were obtained in the on-zone bright-field (BF) imaging condition. $\langle 001\rangle$ cross-sectional samples were also investigated in order to study the size distribution of the dots along the stacking direction. Figure 1 shows a schematic view of the dots in both plan-view (a) and cross-sectional geometry (b). The zone axis as well as the main crystallographic directions are evidenced.

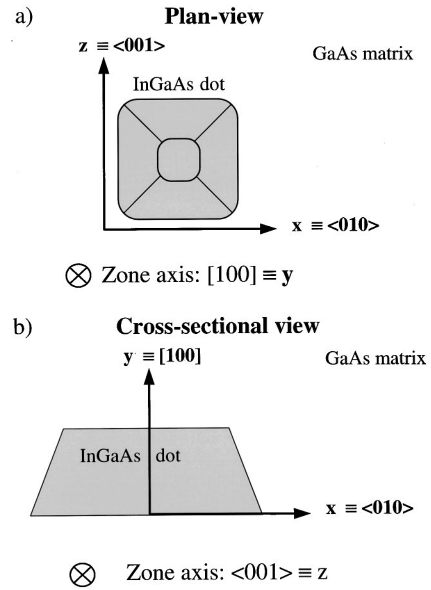

FIG. 1. Schematic view of an $In_{0.5}Ga_{0.5}As$ dot embedded in the GaAs matrix in both plane-view (a) and cross-sectional geometry (b). The zone axis direction used in the TEM observation as well as the main crystallographic directions are evidenced.

III. CRITICAL ISSUES IN THE INTERPRETATION OF PHASE CONTRAST IMAGES

A. Experimental results

Figures 2(a) and 2(b) report the high-resolution images of a single column of six fold stacked dots obtained in the (a) $\langle 001\rangle$ and (b) $\langle 011\rangle$ zone axes, respectively. Both images show the good structural quality of the layers and a good stacking of the dot columns. Besides, relevant differences can be immediately noticed. In the $\langle 011\rangle$ zone axis the dots appear like flat islands, of lens shape, with an average lateral size of about 20 nm and an average height of about 4 nm. Moreover, the dots essentially show only a darker contrast, related both to the heavier In atoms and to the strain field; therefore, an overestimation of the dot size together with an erroneous evaluation of the shape can occur.

Further information about the dot shape can be obtained by a comparison of the HRTEM images in the $\langle 001\rangle$ and $\langle 011\rangle$ zone axes. In the image in Fig. 2(a) the dot shape is more likely to be a truncated pyramid or a truncated cone, as derived both from the mass contrast and from the phase contrast.

In the $\langle 011\rangle$ zone axis, the hexagonal array of the bright spots preserves the same features in both the $In_xGa_{1-x}As$ dots and the GaAs matrix: only slight variations in the relative intensity of the spots can be noticed. Therefore, in spite of the good quality of the high-resolution image, it is not straightforward to extrapolate reliable information about the dot shape. On the contrary, in the $\langle 001\rangle$ zone axis a clear difference in the spot array between the $In_xGa_{1-x}As$ dot and GaAs matrix can be observed. This difference was experimentally maximized by properly adjusting the objective lens defocus. In particular, in the GaAs lattice, the spots are arranged in squares with a slightly weaker spot in the middle; in the $In_xGa_{1-x}As$ lattice the weak spot almost disappears. It follows that in the GaAs matrix the visibility of the 220 lattice fringes (at 45° with respect to the growth direction) is predominant whereas in the $In_xGa_{1-x}As$ dots the 200 lattice fringes, parallel and/or perpendicular to the growth direction, prevail. Therefore it is possible to distinguish between the region where In is confined and the surrounding areas; this allows us to get a more accurate evaluation of the dot dimensions and more reliable information about their shape. As a further remark, it is worth noting that the wetting layer contrast is very faint in the first two layers, where the dot formation process (still at the early stages) has not completely occurred, whereas it almost disappears in the uppermost layers, where the dots are fully developed, indicating a complete migration of the In towards the dots. In our opinion this information, fundamental for the understanding of the electronic behavior of the quantum dots, cannot be obtained with the same accuracy in the $\langle 011\rangle$ zone axis. However, even in this projection much care must be taken in the interpretation

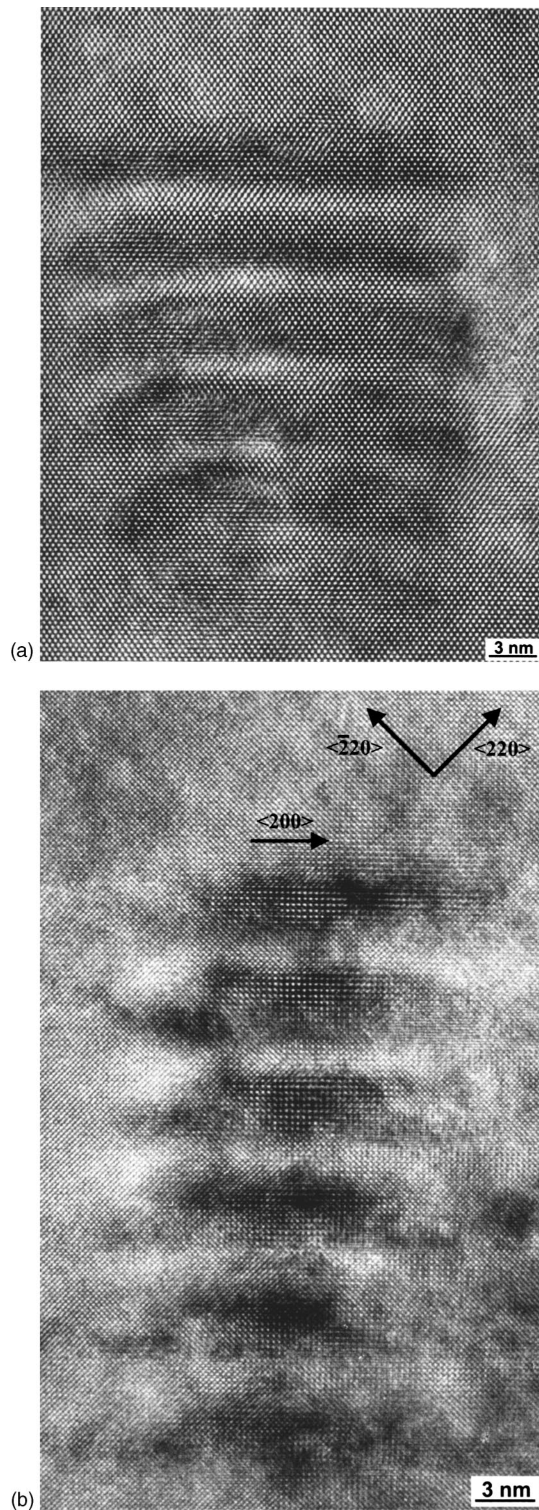

FIG. 2. Experimental HRTEM images of a sixfold stacked $In_{0.5}Ga_{0.5}As$/GaAs quantum dot sample, obtained in the (a) ⟨011⟩ and (b) ⟨001⟩ zone axes.

of the high-resolution image, since the effect of the dot strain field and of the strain relaxation, due to the sample thinning, is always present. For this reason it is extremely difficult to apply quantitative analyses, generally performed on unstrained structures,[25,26] to such images.

B. Discussion

The influence of the composition on the phase contrast in the ⟨001⟩ zone axis is basically due to a particular set of lattice reflections, which are sensitive to the atomic content of the crystal unit cell.[25] In the zinc-blende structure of III-V semiconductors, the chemical information is carried by the 200 reflections, since their intensity is proportional to the square modulus of the difference between the scattering factors of the group-III and group-V elements ($I_{200} \propto |f_{\mathrm{III}} - f_{\mathrm{V}}|^2$). Indeed, it has been recently demonstrated[26] that I_{200} is linearly proportional to the stoichiometric ratio x in ternary alloys such as $In_xGa_{1-x}As$. The contribution of the chemically sensitive reflections to the high-resolution images of III-V semiconductors is maximized by viewing the sample just along the ⟨001⟩ zone axis. Vice versa, in the more commonly used ⟨011⟩ zone axis the contribution of the 200 reflections, which are indeed very faint, is hidden by the 111 reflections ($I_{111} \propto |f_{\mathrm{III}} + f_{\mathrm{V}}|^2$) which are the strongest ones and closest to the transmitted beam.[27]

Since different parameters, such as specimen thickness t and objective lens defocus ε, play an important role in the determination of the phase contrast in high-resolution images, HRTEM simulations were performed by using the Cerius 2 software[28] in order to have theoretical feedback for the experimental results and to check how the experimental conditions influence the effect of the 200 reflections to the HRTEM images.

Under dynamical conditions, the intensity of the 200 reflections depends on the sample thickness:[27] for this reason, a preliminary investigation of the thickness dependence of the 200 beam intensity was carried out by propagating the electron beam through crystal slices of increasing thickness and visualizing the amplitude of the 200 beams. Also, the intensity of the 220 beams was calculated as, in the ⟨001⟩ projection, they mostly contribute to the phase contrast image. The relative weight of the 200 reflections with respect to the 220 ones discriminates the intensity of the compositional signal. Figure 3 reports the plots of the intensities of the 200 and 220 reflections versus thickness, for (a) GaAs and (b) $In_xGa_{1-x}As$ bulk crystals. The $R = 200/220$ intensity ratio is also reported in Fig. 3(c) for GaAs and $In_xGa_{1-x}As$. It is evident that the 220 reflections, which are "structural" reflections, are predominant for GaAs, even oscillating as a function of the thickness. The 200 "chemical" reflections have a stronger intensity for $In_xGa_{1-x}As$. As a result, the plot in Fig. 3(c) shows that, on average, R is higher for $In_xGa_{1-x}As$ than for GaAs. On the basis of these results, HRTEM simulations were performed at two significant sample thicknesses: 175 Å, where R is maximum for $In_xGa_{1-x}As$ and minimum for GaAs, and at 621 Å, where the opposite condition occurs. GaAs and $In_xGa_{1-x}As$ bulk crystals were used for simulations, without taking into account strain effects, since our aim was simply to qualitatively compare the phase contrast of the experimental and simulated images. For each thickness value, through-focus series were obtained by varying the objective lens defocus from −400 Å to +400 Å in order to see how the spatial frequencies of the diffracted beams (200 and 220) are filtered by the

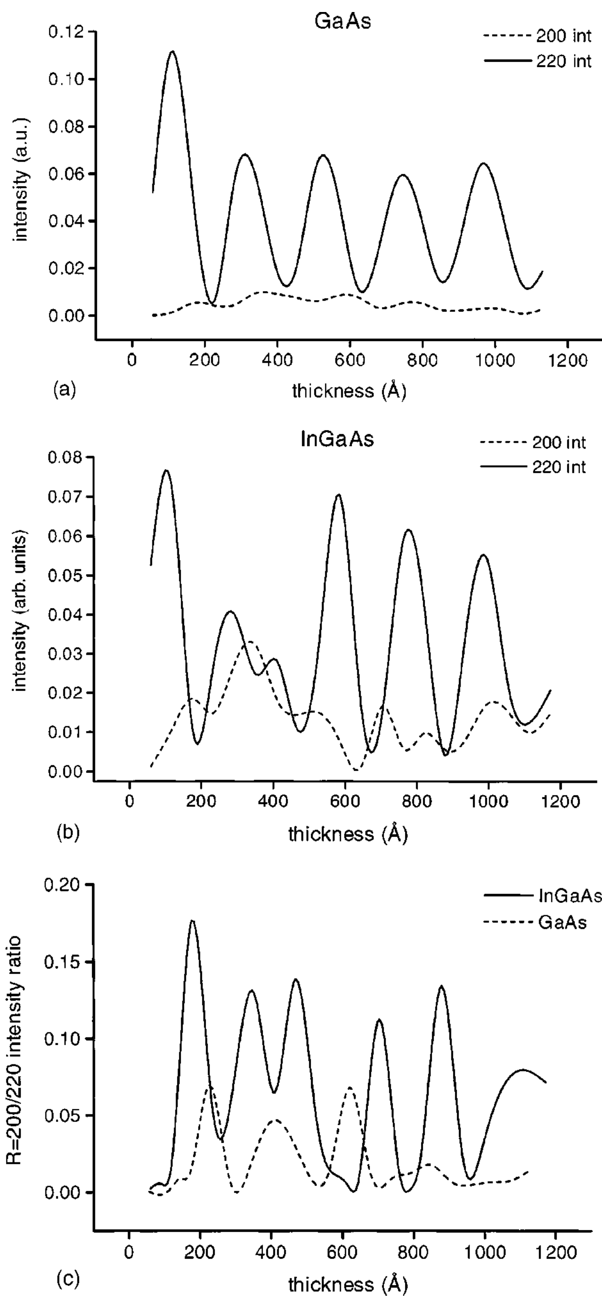

FIG. 3. Plot of the intensity of the 200 and 220 reflections versus crystal thickness for (a) GaAs and (b) $In_{0.5}Ga_{0.5}As$ single crystals; (c) $R=200/220$ intensity ratio versus thickness for GaAs and $In_{0.5}Ga_{0.5}As$.

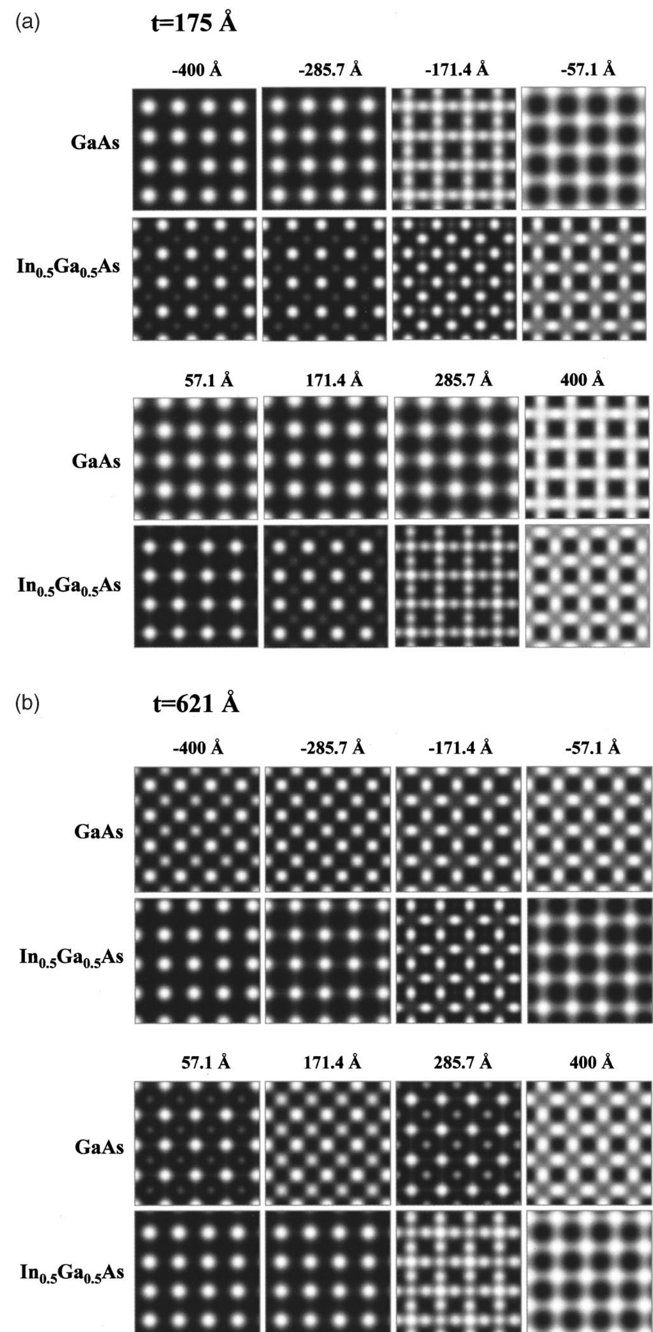

FIG. 4. HRTEM through-focus images calculated for GaAs and $In_{0.5}Ga_{0.5}As$ at crystal thicknesses of 175 Å (a) and 621 Å (b).

electron microscope. These results are reported in Figs. 4(a) and 4(b). The comparison between the GaAs and $In_xGa_{1-x}As$ lattice images clearly shows that for each selected thickness, it is possible to tune the defocus conditions which are most sensitive to the different chemical composition of the two materials (for example, at $t=175$ Å and $\varepsilon=-400$ Å or $\varepsilon=-285.7$ Å and at $t=621$ Å and $\varepsilon=-400$ Å). In particular, at $t=175$ Å and $\varepsilon=-400$ Å the simulated images fit well the behavior of the experimental ones. This should be possible, in principle, at any other thickness value, in the range allowed for high resolution.

Through-thickness simulations (not reported here, for brevity sake) demonstrated that at few specific thickness values [where R is almost the same for GaAs and $In_xGa_{1-x}As$, see the graph in Fig. 3(c)], the difference between GaAs and $In_xGa_{1-x}As$ is not so striking, like in the two cases discussed above. This inconvenience can be, anyway, experimentally solved by moving to an adjacent region of the specimen with a sightly different thickness, which is always available due to the typical wedge shape of TEM specimens.

Since GaAs layers can cover the top and bottom surfaces of the $In_xGa_{1-x}As$ quantum dot, their contribution to the HRTEM images could hide the compositional signal. In or-

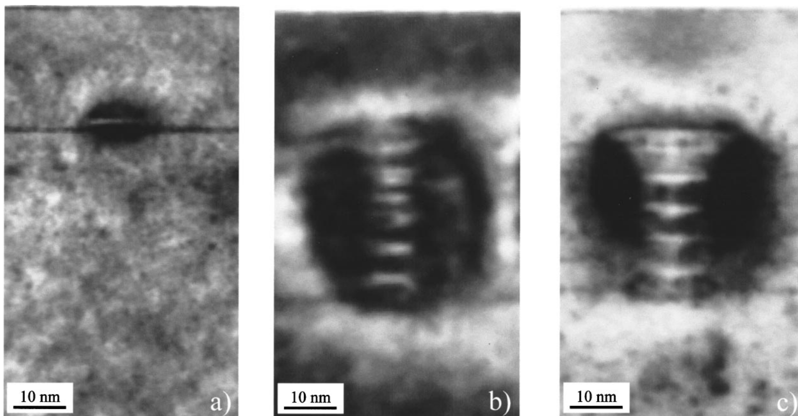

FIG. 5. ⟨001⟩ cross-section TEM images of the single (a), uniform (b), and nonuniform (c) vertically stacked dot sample.

der to check this hypothesis, HRTEM simulations were also obtained from sandwiched structures, consisting of two external GaAs layers and a middle $In_xGa_{1-x}As$ layer; the total thickness of the GaAs layers was chosen equal to about 20 nm, the real thickness of the $In_xGa_{1-x}As$ dots. These simulations were compared to those obtained from a layer of GaAs having the same thickness of the sandwiched structure. The results of these simulations showed that also in this case, closer to the real experimental conditions, it is still possible to distinguish between the heterostructure, containing $In_xGa_{1-x}As$ material, and the pure GaAs.

IV. CORRELATION BETWEEN PLAN-VIEW DIFFRACTION CONTRAST AND STRAIN FIELD

A. Experimental results

In Fig. 5 we show the cross-sectional low-magnification images obtained from three samples, consisting, respectively, of a single (a) and sixfold stacked dot layers [5(b) and 5(c)]. The comparison between the images of the vertically stacked quantum dot samples [Figs. 5(b) and 5(c)] shows that, although the dimensions of the bottomost layers are nearly the same, the situation is quite different for the topmost ones. In particular, the sample in Fig. 5(b) shows dots which are vertically aligned without extended defects and with a rather uniform size (only the topmost dots exhibit a little enlargement). Conversely, the sample in Fig. 5(c) exhibits a strong increase of the dot size. This important difference is related to modified growth conditions that allowed us to improve the quality of the stacked structures in terms of the vertical size uniformity.

As a result, during TEM experiments in plan-view geometry, the transmitted electron beam experiences the effect of the strain fields associated with ''families'' of dots having different sizes along the stack. Figures 6(a), 6(b), and 6(c) show the on-zone plan-view BF images corresponding to the same sequence of samples reported in Fig. 5. The three images show striking differences in the contrast pattern. In particular, for the single dot [Fig. 6(a)] and the rather uniform stacked dots [Fig. 6(b)] the contrast is characterized by an external dark region, of nearly circular shape, with a bright spot at the center. The stacked dots with a nonuniform size along the stack show a completely different feature, i.e., an intensity modulation, resulting in a flowerlike pattern. Figures 6(d), 6(e), and 6(f) display the contrast line scan performed along the ⟨010⟩ directions, i.e., the intensity modulation along the dashed lines in Figs. 6(a)–6(c). A main central maximum is observed in the line-scan profiles of Figs. 6(d) and 6(e) whereas Fig. 6(f) shows three maxima of comparable intensity, the external ones being lightly weaker and symmetric with respect to the central one.

B. Theoretical model

As mentioned before, it is well known that the white and/or black diffraction contrast in the TEM images is due to

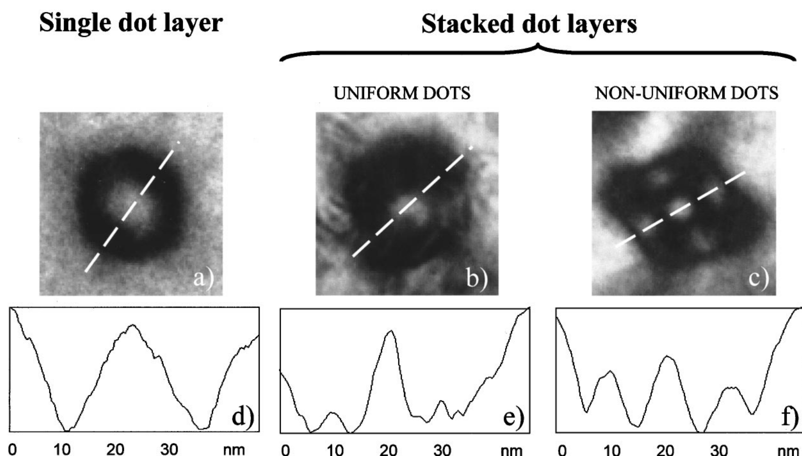

FIG. 6. [100] plan-view images obtained in the on-zone BF imaging conditions from the single (a), uniform (b), and nonuniform (c) vertically stacked dot sample. The contrast line scans, performed along the ⟨010⟩ directions on both images, are also reported (d)–(f).

the inhomogeneous lattice strain associated with the three-dimensional (3D) islands.[29] This induces a local variation of the lattice planes orientation, resulting in a local modification of the electron-diffraction conditions. The different contrast observed in the single and stacked dot samples is a quite general feature observed in many other samples, regardless of the adopted growth conditions. This allows one to hypothesize that the only parameter which affects the contrast pattern of plan-view images is the extent of dot size uniformity along the stacking direction. We believe that the strain field associated with dot families of different sizes overlaps, inducing a modulation of the strain along the stacking direction, which results in a modification of the electron-diffraction condition.

In order to test this hypothesis, we have studied the effect of the linear combination of the strain fields associated with dots of different dimensions. The exact strain field in capped quantum dots is generally calculated with the finite element method. However, at first approximation we assumed it is equal to the strain field felt by quantum dots induced by stressors[30] of simple parallelepiped shape. In this approximation we can calculate the quantum dot strain field by using the analytical method reported in Ref. 31. The strain field calculated in this way is consistent with one obtained with finite element method calculations.

We developed the functions describing the surface profile, $tf(x,z)$ [the stressor pattern, with the $f(x,z)$ periodic function such that $-1<f(x,z)<1$ and t maximum amplitude of the profile modulation] in a Fourier series: the stress tensor $\boldsymbol{\sigma}$ is then calculated by superimposing the stress field associated with each cosine component. Since the amplitude of the relevant Fourier components are much smaller than the corresponding wavelength, we looked for a solution of the elasticity equations

$$(1+\nu)\nabla^2\boldsymbol{\sigma}+\nabla^T\boldsymbol{\nabla}\,\mathrm{Tr}(\sigma)=0, \tag{1a}$$

$$\boldsymbol{\nabla}\cdot\boldsymbol{\sigma}=0, \tag{1b}$$

having the form of a series expansion

$$\boldsymbol{\sigma}(x,y,z)=\sum_{\alpha=0}^{\infty} t^{\alpha}\sigma^{\alpha}(x,y,z), \tag{2}$$

where $\boldsymbol{\nabla}^T$ is the transpose of the gradient vector $\boldsymbol{\nabla}$ and ν is the Poisson's ratio. The boundary conditions are given by the requirement that no net force acts on the free surface $[y=tf(x,z)]$,

$$0=\boldsymbol{\sigma}\boldsymbol{\nabla}[y=tf(x,z)]=\boldsymbol{\sigma}\hat{\mathbf{y}}-t\boldsymbol{\sigma}\boldsymbol{\nabla}f, \tag{3}$$

where $\hat{\mathbf{y}}$ is the unit vector along the positive y direction.

For the same reasons that in Eq. (2) the stress field at the free surface can be expanded in a series around $y=0$, we obtain

$$\boldsymbol{\sigma}[x,tf(x,z),z]=\sum_{\beta=0}^{\infty}\sum_{\alpha=0}^{\infty}\frac{1}{\beta!}t^{\alpha+\beta}f(x,z)^{\beta}\left.\frac{\partial^{\beta}\sigma^{(\alpha)}}{\partial y^{\beta}}\right|_{y=0}, \tag{4}$$

where the derivatives of the stress fields on the right-hand side are calculated at $y=0$. By using the series expansion in Eq. (4), Eq. (3) becomes

$$\sum_{\beta=0}^{\infty}\sum_{\alpha=0}^{\infty}\frac{1}{\beta!}t^{\alpha+\beta}f(x,z)^{\beta}\left.\frac{\partial^{\beta}\sigma^{(\alpha)}}{\partial y^{\beta}}\right|_{y=0}\hat{y}-\sum_{\beta=0}^{\infty}\sum_{\alpha=0}^{\infty}\frac{1}{\beta!}t^{\alpha+\beta+1}f(x,z)^{\beta}\left.\frac{\partial^{\beta}\sigma^{(\alpha)}}{\partial y^{\beta}}\right|_{y=0}\nabla f=0. \tag{5}$$

This is a power series which makes it possible to find the boundary conditions on the plane, $y=0$, at any order in t. Hence by requiring that all the coefficients of the power series are zero a recursive formula is found which provides an explicit form for the boundary condition to be satisfied with the functions $\sigma^{\alpha}(x,y,z)$.

In the case of stressors having a simple parallelepiped shape, the first-order expansion of the hydrostatic component of the stress field is given by $\sigma_{\mathrm{hy}}=t\sigma_{\mathrm{hy}}^{(1)}+\cdots$, where

$$\begin{aligned}\sigma_{\mathrm{hy}}^{(1)}=-\frac{\pi}{6}\sigma_0(1+\nu)\{&\chi_y(z)[\phi_y(-x,z)+\phi_y(x,z)]\\&+\chi_y(-z)[\phi_y(-x,-z)+\phi_y(x,-z)]\\&+\chi_y(x)[\phi_y(-z,x)+\phi_y(z,x)]+\chi_y(x)[\phi_y(-z,-x)\\&+\phi_y(z,-x)]\},\end{aligned} \tag{6}$$

with

$$\phi_y(u,\nu)=\frac{L_u+u}{\sqrt{(L_u+u)^2+(L_\nu+\nu)^2+y^2}},$$

$$\chi_y(u)=\frac{L_u+u}{\sqrt{(L_u+u)^2+y^2}}. \tag{7}$$

L_x and L_z are the dimensions of the dot. In Eq. (6) the stress field diverges along the border of the box where, however, the displacement field is continuous.

The strain tensor ε is then obtained by applying the Hooke's law. With this method we found that the hydrostatic strain component is constant inside the dot region and zero outside. This is consistent with the results obtained by other methods in capped quantum dots.[32,33] A small strain modulation is found at the edges of the dots.

It is worth noting that the displacement vector $\mathbf{u}$ is related to the strain tensor ε by the well-known equation

$$\varepsilon_{ij}=\frac{1}{2}\left(\frac{\partial u_i}{\partial x_j}+\frac{\partial u_j}{\partial x_i}\right). \tag{8}$$

Only the strain components leading to a local variation of lattice planes that are parallel to the electron beam give rise to contrast in the TEM plan-view images, namely, ε_{xx}, ε_{zz}, ε_{xz}, and ε_{zx} [see Fig. 1(b)]. Since the off-diagonal components are smaller than the diagonal terms, in our discussion we consider only the term $\varepsilon_{xx}+\varepsilon_{zz}$.

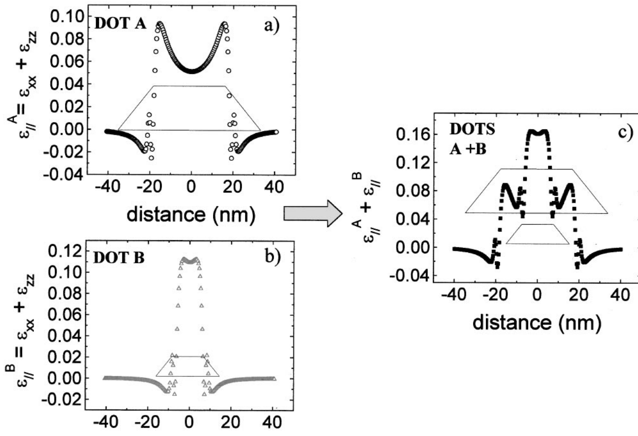

FIG. 7. Plot of the calculated strain components $\varepsilon_{xx}+\varepsilon_{zz}$ for two dots having different sizes along the diagonal direction. The open circles (a) and open up triangles (b) display the strain field of the big (dot A) and small dot (dot B), respectively. The close squares (c) represent the coherent superposition of the strain field associated with dot A and dot B, resulting in a modulation of the strain field.

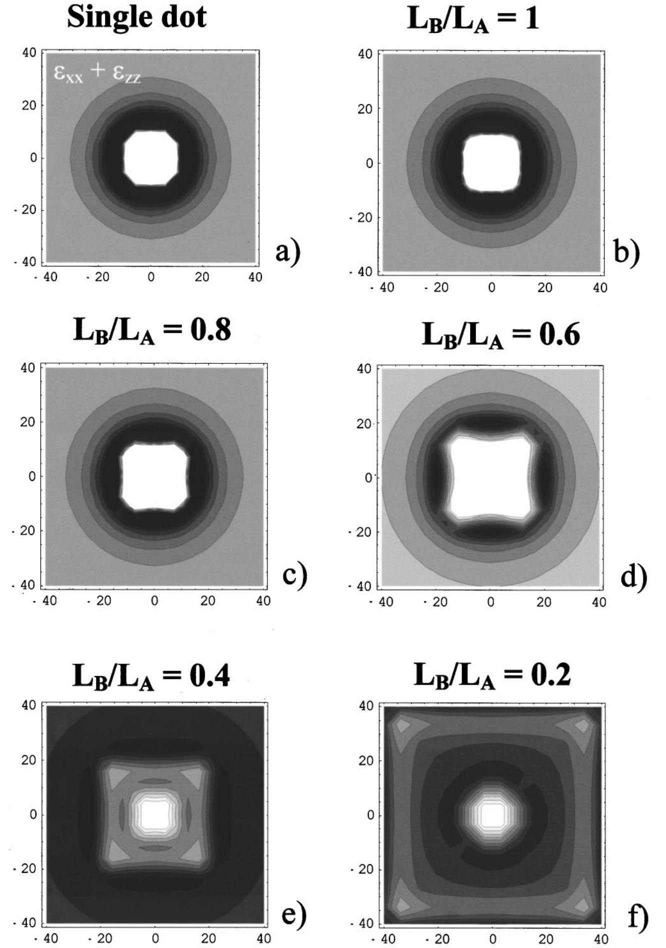

FIG. 8. Contour plot of the calculated strain field ($\varepsilon_{xx}+\varepsilon_{zz}$) for single (a) and vertically stacked quantum dots (b)–(f) as a function of the ratio between the sizes (L_A and L_B) of the two dot families. The superposition between the strain fields associated with each family induces a modulation of the field which becomes more and more evident with increasing the difference in the size of the two families.

Firstly, we considered a simple model with only two stacked quantum dots of different size. We label the bigger dot as ''dot A'' and the smaller dot as ''dot B.'' In Fig. 7 we plot the calculated strain component $\varepsilon_{xx}+\varepsilon_{zz}$ along the diagonal of dots for the two dots. In dot A [Fig. 7(a)], the dilated region is larger than dot B [Fig. 7(b)]. As a consequence, the electrons transmitted at the center of the stacked quantum dots (around $x=z=0$) feel a strain dilatation in both quantum dots, whereas the electrons at the edges of the dots (at about 15 nm far from the center) feel a strain dilation in dot A and a strain compression in dot B. The resulting strain field felt by the electrons is the coherent superposition of the strain fields associated with the two dots [Fig. 7(c)]. A main maximum occurs at the center of the structure due to the combination of the strain field related to expanded regions [Figs. 7(a) and 7(b)], whereas the secondary maxima are generated by the combination of regions where the structure is expanded (in the bigger dot A) and regions where the structure is compressed (in the smaller dot B). It follows, therefore, that the combination of strain fields associated with dots of different dimensions (the size of dot A is approximately twice that of dot B) induces a modulation of the strain [Fig. 7(c)] which results in a correspondent modulation of the electron-diffraction conditions.

At this point it is interesting to analyze how such a modulation changes as a function of the size of the two dots (L_A and L_B). In Figs. 8(a) and 8(b) we display the calculated contour plot of $\varepsilon_{xx}+\varepsilon_{zz}$ for a single and two stacked dots of same dimension. The white and black zones correspond, respectively, to expanded and compressed regions, whereas the different gray-scale zones display intermediate conditions. As expected, in the single dot [Fig. 8(a)] strain dilation is observed into the island whereas strain concentration occurs at the edges. As a consequence, the transmitted electron beam is diffracted in a different way at the center and at the edges of the quantum dots resulting in the diffraction contrast of Fig. 6(a). Therefore, for $L_A=L_B$, the contour plot of the two vertically stacked layers coincides with that of the single dot [Fig. 8(a)], since, in this case, we have the coherent superposition of strain fields associated with quantum dots having the same size, so that no superposition between expanded regions and compressed regions occurs. When the ratio L_B/L_A decreases [Figs. 8(c)–8(f)], i.e., when the difference between the dot dimensions of the two families increases, the modulation of the strain field becomes evident. A flowerlike pattern is found only for $L_B/L_A \leq 0.5$. This suggests that in the study of vertically stacked dot samples, the plan-view diffraction contrast can be used to obtain information about the uniformity of the dot sizes along the stacking direction. This is fundamental to fabricate a quantum dot laser of high quality.

Our model is readily extended to the real case of Fig. 5(c) in which the sample consists of six dot layers whose size changes continuously from the bottom to the top layers. A realistic calculation was performed by employing two six-

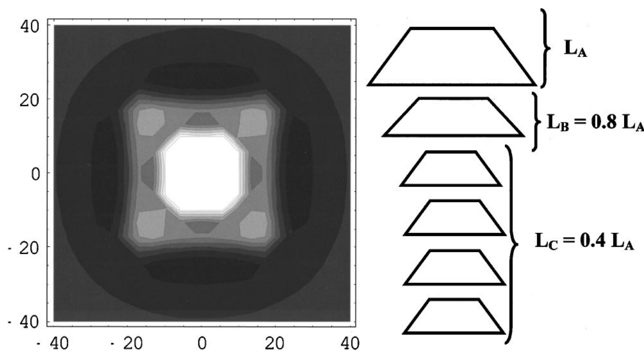

FIG. 9. Contour plot of the calculated total strain field ($\varepsilon_{xx}+\varepsilon_{zz}$) for a six-layer model. We considered the dot dimensions such that $L_B=0.8L_A$ and $L_C=0.4L_A$.

layer models. We assumed three dot families A, B, and C with $L_B=0.8L_A$ and $L_C=0.4L_A$ (Fig. 9). We found again a strain modulation in which we can distinguish a central maximum and four weaker secondary maxima.

It is clear that the calculated strain patterns are not perfectly identical to the TEM contrast. The remote areas surrounding the dots are dark in the strain field contour plots, reflecting a small strain intensity, whereas the corresponding areas in the TEM images are bright. This is not surprising because in one case we look at a strain pattern and in the other case at a diffraction contrast. However, the goal of our model is to show that the coherent superposition of strain fields associated with quantum dots of different sizes induces a modulation of the total strain field that must result necessarily in a modulation of the electron-diffraction contrast.

V. CONCLUSIONS

High-resolution transmission electron microscopy is a suitable investigation tool for the characterization of quantum dot structures when all its potentialities are properly used. Among these, the possibility of viewing heterostructure materials at a nearly atomic resolution with useful chemical information is very suitable for the observation of quantum dot systems. In particular, we demonstrate how misinterpretations in the evaluation of the actual shape of the dots can occur when HRTEM investigations are performed only in the $\langle 011\rangle$ zone axis. Moreover, we explore the influence of many experimental parameters to assess the general validity of the chemically sensitive HRTEM investigations for the case $In_xGa_{1-x}As$ quantum dot buried in a GaAs matrix.

The results of the calculations developed in Sec. IV are found to describe, even though in a qualitative way, the strain modulation of single and sixfold stacked dots with a surprisingly good accuracy, elucidating the diffraction contrast observed in the plan-view TEM images of our samples. A more quantitative analysis would require advanced simulations of the TEM images in which the modeled strain field is used as an input for the dynamical electron scattering.[11,14,17,18] This is a very complicated issue to address due to the complex structure of our samples. Nevertheless our experimental observations and theoretical results suggest that the different diffraction contrast can be due to a coherent superposition of the strain fields associated with dots of different sizes. This induces a modulation of the total strain field, resulting in a modification of the electron-diffraction conditions. Therefore, from the plan-view diffraction contrast we can get information about the uniformity of the dots in the stack and of the variations of their relative sizes.

ACKNOWLEDGMENTS

This work has been supported by INFM through PRA-SSQI. One of the author (A.T.) would like to acknowledge the Istituto CNR-IME of the Consiglio Nazionale delle Ricerche for the partial support of this work during her Ph.D. course.

*Corresponding author. Email: antonietta.taurino@ime.le.cnr.it

[1] C. Weisbuch and G. Vinter, in *Quantum Semiconductor Structures* (Academic, Boston, 1991).
[2] R. Rinaldi, R. Mangino, R. Cingolani, H. Lipsanen, M. Sopanen, J. Tullky, M. Brasken, and J. Ahopelto, Phys. Rev. B **57**, 9763 (1998).
[3] N. N. Ledentsov, Solid-State Electron. **40**, 785 (1996).
[4] R. Rinaldi, Int. J. Mod. Phys. B **12**, 471 (1998).
[5] G. S. Solomon, J. A. Trezza, A. F. Marshall, and J. S. Harris, Phys. Rev. Lett. **76**, 952 (1996).
[6] A. Endoh, Y. Nakata, Y. Sugiyama, M. Takatsu, and N. Yokoyama, Jpn. J. Appl. Phys., Part 1 **38**, 1085 (1999).
[7] Y. Arakawa, 23rd *International Conference on the Physics of Semiconductors* (World Scientific, Singapore, 1997), Vol. 2, p. 1349.
[8] M. De Giorgi, A. Vasanelli, R. Rinaldi, M. Anni, M. Lomascolo, S. Antonaci, A. Passaseo, R. Cingolani, A Taurino, M. Catalano, and E. Di Fabrizio, Micron **31**, 55 (2000).
[9] S. Ruminov and K. Scheerschmidt, Phys. Status Solidi A **150**, 471 (1995).
[10] J. Zou, X. Z. Liao, D. J. H. Cockayne, and R. Leon, Phys. Rev. B **59**, 12 279 (1999).
[11] X. Z. Liao *et al.*, Phys. Rev. B **58**, R4235 (1998).
[12] D. Leonard *et al.*, J. Vac. Sci. Technol. B **12**, 1063 (1994).
[13] S. Ruvimov *et al.*, Phys. Rev. B **51**, 14 766 (1995).
[14] N. N. Ledentsov *et al.*, Appl. Phys. Lett. **70**, 2888 (1997).
[15] G. D. Lian, J. Yuan, L. M. Brown, G. H. Kim, and D. A. Ritchie, Appl. Phys. Lett. **73**, 49 (1998).
[16] K. Georgsson, N. Carlsson, L. Samuelson, W. Seifert, and L. R. Wallenberg, Appl. Phys. Lett. **67**, 2981 (1995).
[17] K. G. F. Janssens *et al.*, Appl. Phys. Lett. **67**, 1530 (1995).
[18] T. Benabbas, P. Francois, Y. Androussi, and A. Lefebvre, J. Appl. Phys. **80**, 2763 (1996).
[19] D. Jacob *et al.*, J. Cryst. Growth **179**, 331 (1997).
[20] Y. Androussi, T. Benabbas, and A. Lefebvre, Philos. Mag. Lett. **79**, 201 (1999).
[21] X. Z. Liao *et al.*, Phys. Rev. Lett. **82**, 5148 (1999).
[22] H. J. Lee *et al.*, J. Cryst. Growth **172**, 18 (1997).
[23] L. De Caro, A. Giuffrida, E. Carlino, and L. Tapfer, Acta Crystallogr., Sect. A: Found. Crystallogr. **53**, 168 (1997).

[24] A. Passaseo, A. L. Convertino, M. Longo, R. Rinaldi, S. Antonaci, R. Cingolani, A. Taurino, and M. Catalano, J. Appl. Phys (to be published).

[25] A. Ourmazd, F. H. Baumann, M. Bode, and Y. Kim, Ultramicroscopy **34**, 237 (1990).

[26] G. Mountjoy *et al.*, Appl. Phys. Lett. **71**, 950 (1997).

[27] P. Hirsch *et al.*, *Electron Microscopy of Thin Crystals* (Robert E. Krieger Publishing Co., Inc., 1977).

[28] CERIUS Molecular Modeling Software for Material Research from Molecular Simulation Inc. of Burlington, MA, and Cambridge, UK.

[29] J. Y. Yao, T. G. Andersson, and G. L. Dunlop, J. Appl. Phys. **69**, 2224 (1991).

[30] J. Tulkki and A. Heinämäki, Phys. Rev. B **52**, 8239 (1995).

[31] M. Mazzer, M. De Giorgi, R. Cingolani, G. Porello, F. Rossi, and E. Molinari, J. Appl. Phys. **84**, 3437 (1998).

[32] C. Pryor, J. Kim, L. W. Wang, A. J. Williamson, and A. Zunger, J. Appl. Phys. **83**, 2548 (1998).

[33] A. D. Andreev, J. R. Downes, D. A. Faux, and E. P. O'Reilly, J. Appl. Phys. **86**, 297 (1999).